



DIRECTION-DEPENDENT ANALYSIS OF PARAMETERS FOR STOCHASTIC SYNTHESIS OF VERTICAL GROUND MOTION

Zelin Cao⁽¹⁾, Xiaxin Tao⁽²⁾

⁽¹⁾ PhD candidate, School of Civil Engineering, Harbin Institute of Technology, Harbin 150090, China, zlcao@hit.edu.cn

⁽²⁾ Professor, School of Civil Engineering, Harbin Institute of Technology, Harbin 150090, China, taoxiaxin@aliyun.com

Abstract

For synthesis of tridimensional ground motions, the available deterministic approach is no longer efficient in high frequency range (say, >1 Hz) for computational limitation and limited knowledge on small-scale heterogeneity in the regional crust, while the widely adopted stochastic synthesis, up to now only working for unidirectional horizontal record, needs to be developed further for vertical component. A research on the direction-dependence of key seismic parameters in the stochastic method, such as stress parameter, quality factor, radiation pattern, kappa factor and site amplification, is presented in this paper to evaluate the different effects of crustal inhomogeneity on vertical and horizontal components. The result indicates that the first two are just region-specific parameters of the crust medium property and status, whereas the other three are complicatedly and strongly direction-dependent. Then, we incorporate the direction-dependent pattern based on Pulido's research for an accurate energy distribution of wave radiated from the source, and take the difference between vertical and horizontal kappa factor and site amplification into account. Vertical ground motions for the 1994 Northridge earthquake are synthesized with these improvements, and the comparisons with the observed motions show reasonable agreement in average, which is followed by further validation to demonstrate the accordance with the recently developed vertical ground motion prediction equations.

Keywords: stochastic synthesis; vertical ground motion; Northridge earthquake; radiation pattern; site amplification



1. Introduction

Vertical ground motion, as compared with its horizontal counterpart, is often not well considered in the seismic design from the general perspective that structural damage caused by vertical earthquake action is little due to relatively smaller intensity of ground motion and larger bearing redundancy of structures in the vertical direction. Nowadays, besides critical structures like nuclear power plants and dams, standard short-period structures close to active faults like ordinary highway bridge [1, 2] are also found to be significantly affected by vertical ground motion. Furthermore, earthquake damage surveys [3, 4] show multiple occurrences of structural damage caused by vertical motion. Therefore, proper prediction of vertical ground motion becomes an important issue.

The vertical-to-horizontal spectral ratios (V/H) are typically used to understand and quantify the characteristics of vertical ground motion. Various studies [5, 6, 7] reveal that V/H is primarily a function of natural period and distance, generally exhibiting higher ratios at short periods or on soft sites. From this, it is easy to find the deficiency in the regulations of seismic codes in many countries (e.g., China [8] and New Zealand [9]) that vertical response spectrum is obtained by scaling the horizontal counterpart with a constant V/H usually between 0.5 and 0.7, even for those pioneering codes such as Eurocode 8 [10] and FEMA P-750 [11]. Additionally, for predication of vertical motion, another alternative is using the vertical ground-motion prediction equations (GMPEs) usually obtained by two approaches: (1) developing vertical GMPEs directly following the same approach for the horizontal ones, such as the vertical GMPEs recently developed by PEER NGA-West2 project [12]; (2) scaling the horizontal GMPEs by the V/H ratio GMPEs [2, 7, 13]. Nevertheless, the application of GMPEs is narrowed by its empirical and regional characteristics. Furthermore, relative to the complexity of earthquake ground motion, GMPEs actually make great simplifications in the expression of the effects of source, path and site, which is believed to cause some deviation in the estimation of ground motions, especially for great earthquake or near-field ground motion.

Synthetic seismogram is an efficient way to predict the expected ground motions for future moderate-to-large damaging earthquakes, which can meet various engineering needs. For synthesis of both vertical and horizontal ground motions, deterministic methods, such as three-dimensional finite-difference method (e.g., Olsen et al. [14]), are effective ways containing a theoretically rigorous representation of fault rupture and wave propagation effects. However, their applicability to high frequency (say, >1 Hz) ground motion prediction is hampered by computational limitations and limited knowledge on small-scale heterogeneity in the regional crust. Recently, hybrid methods (e.g., Pitarka et al. [15]; Graves and Pitarka [16]) are employed to compute the low and high frequency wave fields separately and then combine the two to form broadband seismograms. Nevertheless, the methods for generation of high frequency ground motions, including the widespread stochastic approach [17, 18], up to now only works for unidirectional horizontal record and needs to be developed further for vertical component for the future use in linear and nonlinear antiseismic analysis and risk assessment.

According to Beresnev, et al. [5], vertical motions can be modeled as nonvertically propagating SV waves for most practical applications and shear waves dominate the vertical motions at frequencies up to approximately 10 Hz, suggesting the potential ability of the stochastic method to express vertical ground motion. For extension of the stochastic synthesis, detailed investigation of the direction-dependence of key seismic parameters in the stochastic method, such as stress parameter, quality factor, radiation pattern, kappa factor and site amplification, is presented to evaluate the different effects of crustal inhomogeneity on vertical and horizontal components. Subsequently, we specify the vertical values for direction-dependent parameters in the stochastic method. Finally, vertical ground motions for the 1994 Northridge earthquake are simulated and then compared with observed records and vertical GMPEs for validation.

2. Direction-dependent analysis and improvements of stochastic method

The stochastic finite-fault method (Beresnev and Atkinson [19]; Motazedian and Atkinson [20]) is one of the most powerful methods for simulating the ground motions at high frequencies of engineering interest, which



divides the finite-fault into a number of small sub-faults. Each sub-fault is regarded as a point source, and the Fourier amplitude spectrum (FAS) of ground motion from a point source at a given site [18] can be written as

$$Y(M_0, R, f) = C \cdot S(M_0, f) \cdot P(R, f) \cdot T(f) \cdot I(f) \quad (1)$$

in which C is the scaling factor, $S(M_0, f)$, $P(R, f)$ and $T(f)$ represent the effect of source, path and site, respectively, $I(f)$ is an indicator for the ground-motion type and has apparent independence of direction. Additionally, M_0 , R and f are the seismic moment, the hypocentral distance and frequency, respectively.

2.1 Radiation pattern

The scaling factor in Eq. (1) expresses the energy distribution of seismic wave originating from source in different directions, which can be expanded as

$$C = \frac{R_{\theta\varphi} V F_S}{4\pi\rho\beta^3 R_0} \quad (2)$$

where $R_{\theta\varphi}$ is radiation pattern calculated following Sandeep et al. [21], and the subscript φ is the source-site azimuthal angle measured clockwise from North while θ is the take-off angle of departing seismic ray measured from the downward vertical (see Aki and Richards [22], for detail), F_S is the amplification effect of free surface, generally valued as 2.0, V represents the partition of total shear-wave energy into single component and should be 1 rather than $1/\sqrt{2}$ if $R_{\theta\varphi}$ is valued for one exact direction, ρ and β represent the shear wave velocity and the density of crust, R_0 is the reference distance, generally preferable to 1 km. For a given site, all terms other than $R_{\theta\varphi}$ are exact values, which means that the study of scaling factor can change into that of radiation pattern.

The radiation pattern theory proposed by Ben-Menahem [23] is aimed at reflecting seismic radiation pattern and the source-site azimuthal effect. Boore and Boatwright [24] calculate RMS values of radiation pattern for three typical rupture types within different distances, among which the S-wave RMS of 0.55 for the near-field vertical strike-slip fault is widely used as a constant radiation pattern. The choice of the average value for radiation pattern makes scaling factor a regional constant and loses important opportunity to express different components. While for a given site, theoretical $R_{\theta\varphi}$ of SV- and SH-waves should be generally different from each other, and thus a significant difference will be also existed between vertical and horizontal $R_{\theta\varphi}$, suggesting the dependence on direction and key role to express direction. Therefore, we employ the direction-dependent radiation pattern model R_p for vertical motion based on Pulido's researches [25, 26, 27], as shown below

$$R_p(\theta, \varphi, f) = \begin{cases} F & \text{for } f \leq f_1 \\ F + \frac{f - f_1}{f_2 - f} (F_{ave}/\sqrt{2} - F) & \text{for } f_1 < f < f_2 \\ F_{ave}/\sqrt{2} & \text{for } f \geq f_2 \end{cases} \quad (3)$$

where R_p is set with a lower limit of 0.2 after Boore and Boatwright [24] to avoid very small theoretical value, F denoting $F(\varphi_s, \delta, \lambda, \theta, \varphi)$ is the vertical theoretical radiation pattern in terms of geographical coordinates (here only vertical direction is used) obtained by adding the projections of those of SV- (F_{SV}) and SH-waves (F_{SH}) of a double couple with strike φ_s , dip δ and rake λ , at receiver with take-off angle θ and azimuth φ [22]. And the specific transformation equation for vertical direction is shown below

$$F = |F_{SV} \sin \theta| \quad (4)$$

F_{ave} in Eq. (3) is the average radiation pattern, calculated by the approach of Boore and Boatwright [24] for all rays departing in the specific takeoff angle corresponds to the near field, shown as follows



$$F_{ave} = \left(\sum_{i=SV,SH} \frac{\int_{2\pi/3}^{\pi} \int_0^{2\pi} F_i^2 \sin \theta d\varphi d\theta}{\int_{2\pi/3}^{\pi} \int_0^{2\pi} \sin \theta d\varphi d\theta} \right)^{\frac{1}{2}} \quad (5)$$

In the present work, two frequency thresholds f_1 and f_2 in Eq. (3) have been taken as 1 and 3 Hz, respectively. As presented by Pitarka et al. [15], the first value is from the fact that the deterministic approach to modeling underground structure and the source process is usually reliable at low frequencies (below 1 Hz), while the second value is based on the frequency dependence of the coherence of the radiation pattern analyzed by Liu and Helmberger [28]. This setup of radiation pattern model is based on the fact that the radiation pattern at high frequencies does not follow the theoretical radiation pattern of a double-couple, which is confirmed by multiple researches on different earthquakes [29, 30, 31]. What's more, the analysis of near-field records from different earthquakes have shown that the radiation pattern at the intermediate frequency range is not purely stochastic but is characterized by a transition from the theoretical double-couple radiation pattern at low frequencies to a complete stochastic isotropic radiation pattern at high frequencies.

2.2 Source effect

A simple ω^2 source spectrum model defined by Brune [32] is widely used to describe the shape of source spectrum, as shown below for an example

$$S(M_0, f) = \frac{M_0}{1 + (f/f_c)^2} \quad (6)$$

where f_c is the corner frequency and calculated from

$$f_c = 4.9 \times 10^6 \beta (\Delta\sigma/M_0)^{1/3} \quad (7)$$

where $\Delta\sigma$ is the stress parameter which significantly influences ground motion amplitudes and higher frequency part of FAS. From the conceptual nature, stress parameter is originally defined as a measure of slip relative to fault dimension with a direct physical meaning [33]. Thus, as a parameter to describe the characteristic of earthquake source, stress parameter is independent of direction.

Consequently, as the representation of the point source, $S(M_0, f)$ describes the amplitude through the total energy, and expresses frequency components of wave scattered from the point source, which is only related to the total energy released from the source and two regional parameters, β and $\Delta\sigma$. Therefore, there has no connection between the source effect and the direction of energy scattering.

2.3 Path effect

In the stochastic method, the path effects are modeled by multiplication of geometrical spreading and anelastic attenuation in the frequency domain [18] as expressed below

$$P(R, f) = G(R) \cdot \exp(-\pi fR/Q(f)\beta) \quad (8)$$

where $G(R)$ is the distance-dependent geometrical spreading function, the exponential term is the anelastic attenuation function, and $Q(f)$ is the frequency-dependent quality factor. From the original measurement for shear-waves [34], quality factor presents a clear regional dependence, while no correlations with direction. Thus, regardless of lateral inhomogeneity and anisotropy of the crustal medium, anelastic attenuation function only increases with distance for given frequency and is also irrelevant to direction.

Due to trade-off between the geometric spreading and anelastic attenuation, the geometrical spreading function is often constrained as a trilinear model following Atkinson and Boore [35] to consider the presence of the surface waves within certain distances, in which the model parameters are regional parameters obtained by inversion or regression analyses. Thus, it is evident that geometrical spreading function is mainly independent of



direction because we often ignore the possible influence of different types of seismic wave on the amplitude of three components at different distances.

2.4 Kappa factor

Site effects is the product of site amplification function $A(f)$ and the diminishing function $E(f)$, shown as

$$T(f) = A(f) \cdot E(f) \quad (9)$$

The diminishing function, characterizing the path-independent loss of energy, is shown as

$$E(f) = \exp(-\pi\kappa_0 f) \quad (10)$$

where κ_0 is the zero-distance kappa factor, as introduced by Anderson and Hough [36], and is applied as a low-pass filter to constrain high frequencies, affecting peak ground motion and spectra shape (see Fig.12 in [18], for detail). The kappa value can be determined from the slope fitted to the high frequency part of FAS plotted in log-linear scale [36], or calculated by more recent estimation approaches outlined in Ktenidou et al. [37].

Undoubtedly, exponential decay at high frequencies is also a general feature of vertical ground motion composed primarily of S-wave, as depicted above. However, there are very few researches on vertical kappa despite its potential use in stochastic simulation (Motazedian [38]). Here, several available studies regarding estimates of both horizontal and vertical κ_0 , denoted by $\kappa_{h,0}$ and $\kappa_{v,0}$, respectively, are shown in Table 1 for various regions. It is noteworthy that $\kappa_{v,0}$ is systematically lower than $\kappa_{h,0}$ at all the regions for each site condition, indicating that vertical motions are affected less by the local site conditions, which is also confirmed by the observation of Ktenidou, et al. [42] that the ratio of $\kappa_{h,0}/\kappa_{v,0}$ is around 1 in the borehole and 1.4 at the surface. Generally, for a given region, both $\kappa_{h,0}$ and $\kappa_{v,0}$ decrease as site becomes harder, as we expected from the fact that harder sites will have lower attenuation of high frequency ground motion.

Table 1 – Estimates of both vertical and horizontal kappa values for various regions

Region	Site condition	Vertical value	Horizontal value
Northern Iran [38]	Rock	0.03	0.05
Wenchuan, China [39]	Soil (for most)	0.00855	0.01288(NS)/0.01881(EW)
Northeastern India [40]	Soft rock	0.013	0.025
	Firm ground	0.033	0.041
Northwestern Turkey [41]	C (NEHRP)	0.0150	0.0377
	D (NEHRP)	0.0271	0.0455

In fact, as Askan et al. [41] presents, any significant variation between $\kappa_{v,0}$ and $\kappa_{h,0}$ points out different attenuation of higher frequencies for the vertical and horizontal motions. This observation indeed augments the idea that the kappa factor is significantly affected by site condition in different directions. Therefore we conclude that separate value for vertical kappa should be considered in stochastic simulation.

For the areas lack of site-specific data, $\kappa_{h,0}$ can be inferred from available V_{S30} (the time-averaged shear wave velocity in the top 30 m of the site) from various alternative correlations, as summarized and compared by Ktenidou et al. [37]. However, it is hard to construct a stable relationship of $\kappa_{v,0}$ to V_{S30} so far due to limited of available researches on $\kappa_{v,0}$. Thus, we choose a practical way to obtain $\kappa_{v,0}$ by scaling region-specific $\kappa_{h,0}$. The value of $\kappa_{h,0}$ for California is 0.05 from the observations (Anderson and Hough [36]), and the ratio of $\kappa_{h,0}/\kappa_{v,0}$ is taken as 1.4 from Ktenidou, et al. [42]. Finally, we take the value of $\kappa_{v,0}$ as 0.035 in the following parts.



2.5 Site amplification function

For the other term in Eq. (9), the site amplification function can significantly affect earthquake ground motion. Generally, vertical site amplification is quite different from the horizontal one, and therefore the incorporation of proper vertical site amplification function into the stochastic method is necessary for reliable estimation of the vertical ground motion.

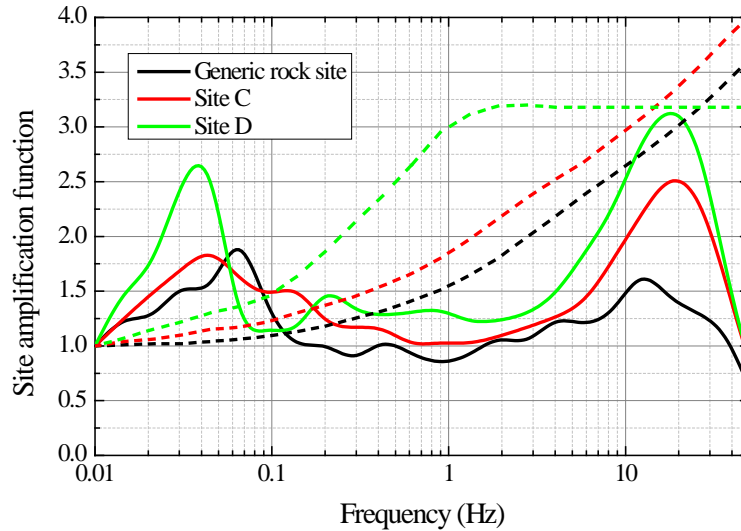


Fig. 1 – Vertical amplification functions (solid lines) for sites C and D (NEHRP) and generic rock site. The corresponding horizontal amplification functions (short dash lines) for sites C and D (Boore and Joyner [45]) and generic rock site with V_{S30} of 760 m/s (Boore [46]) are also plotted for comparison. And the difference between vertical and horizontal kappa factor is set as 0.015 for depicting vertical amplification function.

Note that site amplification function in Eq. (9) is modeled for FAS instead of pseudospectral accelerations (PSA). Although the 5% damped PSA of seismic record have a spectral shape similar to that of FAS (Zhao et al. [43]), it is believed that the ratio of the 5% damped PSA at any site condition to generic rock site (available from vertical GMPEs [44]) has some difference with that of FAS, especially at very short periods, which is unbeneficial for precise simulation of ground motions. Therefore, we prefer to adopt vertical site amplification functions of FAS for sites C and D (NEHRP) and generic rock site, as shown in Fig.1. It is noteworthy that the vertical amplification function is obtained by correcting the horizontal counterpart with an empirical correction factor estimated from three-dimensional seismic observations, as we will propose in an upcoming paper.

3. Validation by Northridge earthquake

In this part, the 1994 Northridge earthquake is chosen as an example for validation. From the PEER NGA-West2 database (Ancheta et al. [47]), all stations with vertical observation in this earthquake other than those located on island or dam are selected for inversion, and the corresponding Record Sequence Numbers in the database are from 942 to 1098 with exclusion of 943, 1050, 1051 (located on island or dam) and 973, 994, 1009, 1010, 1048, 1068, 1078, 1081 (without vertical record). In total, the epicenter distances of all the selected 146 stations ranges from 4.9 to 154.4 km while V_{S30} from 160 to 1222 m/s. Fig.2 shows the epicenter and distribution of the stations. For space reasons, further details of the stations and corresponding records are not repeated herein but can be found in the PEER NGA-West2 database by the unique Record Sequence Number.

In the current study, the modified EXSIM code is used for stochastic simulation. We adapt the finite-fault slip model from Wald et al. [48] with the dimension of $18 \times 24 \text{ km}^2$ for the finite fault and $1.29 \times 1.71 \text{ km}^2$ for the subfaults. The hypocenter is located at 34.213°N , 118.537°W with a fault depth of 5 km. All these parameters of



source model are adopted from the website eQuake-RC. The stress parameter of 50 bars, the frequency-dependent $Q(f)$ model of $180f^{0.45}$, the shear-wave velocity of 3.7 km/s and 0.8 times of it as the rupture velocity, and the density of 2.8 g/cm^3 are applied following Beresnev and Atkinson [49], while the trilinear geometrical spreading function and the distance-dependent duration is modeled after Atkinson and Boore [35] and Beresnev and Atkinson [50], respectively. The kappa factor, site amplification function and radiation pattern are all taken from the discussion above to consider the direction-dependence. The various model parameters used in the stochastic simulation are summarized in Table 2.

Fig. 2 – The epicenter (open star) and distribution of the stations (grey triangles)

Table 2 – Parameters used in the stochastic simulation

Model Parameter	Value or Form
Moment magnitude	6.8
Epicentral latitude and longitude	34.213°N, 118.537°W
Focal mechanism and fault depth	strike 122°, dip 40°, rake 101°, 5 km
Dimension of finite-Fault and subfault	18×24 km ² , 1.29×1.71 km ²
Slip distribution	Wald et al. [48]
Stress parameter	50 bars
Quality factor	$180f^{0.45}$
Window function	Saragoni-Hart
Pulsing percentage	50%
Geometrical spreading	$1/R$ (<70 km), $1/R^0$ (70-130 km), $1/R^{0.5}$ (>130 km)
Crustal density and shear-wave velocity	2.8 g/cm^3 , 3.7 km/s
Rupture velocity	$0.8 \times$ shear-wave velocity



Distance-dependent duration	T_0+bR , $b=0$ (<10 km), 0.16 (10-70 km), -0.03 (70-130 km), 0.04 (>130 km)
Kappa factor, site amplification and radiation pattern	From the previous discussion

Vertical ground motions for the 1994 Northridge earthquake are synthesized using the stochastic finite fault method. For each station, we generate 30 realizations with PSA for 5% damping and the records which minimize the PSA bias to their averages over the period range from 0.01 to 10 s are selected as the final result. Then, direct comparisons are made between observed and simulated PGA, PGV and PSA below.

The residual for ground motion measures (PGA or PGV) at i th station is defined as

$$Residual(i) = \ln OP(i) - \ln SP(i) \tag{11}$$

where OP is the observed peak value recorded in the PEER NGA-West2 database, and SP is the simulated peak value deduced from synthesized histories. A perfect match between the observation and simulation would have *Residual* of 0, whereas a positive residual shows underestimation or vice versa. The residuals for PGA and PGV with respect to V_{S30} are plotted in Fig.3. It can be seen that the simulated and the observed PGA and PGV are in fair agreement with generally unbiased residuals in term of V_{S30} , which proves the feasibility of the adopted site amplification models. Also shown in Fig.3 is the V_{S30} boundary of different site classes (NEHRP). Totally, there are only 2 and 1 stations belong to sites B and E while 62 and 81 for sites C and D.

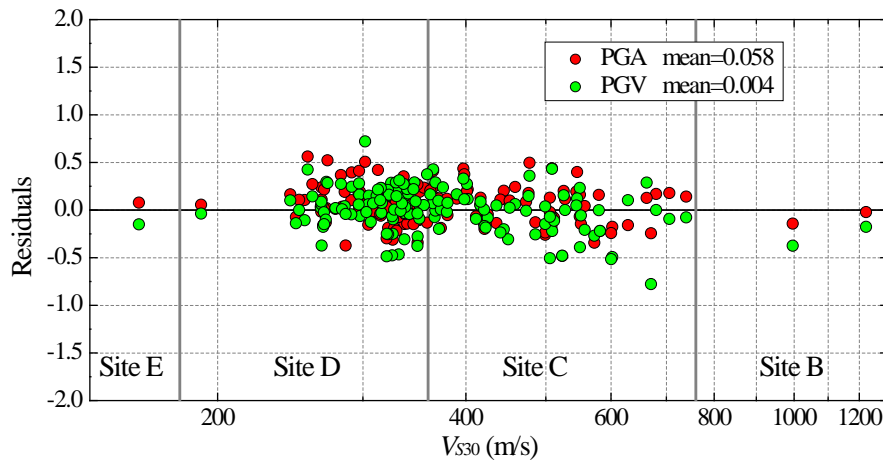


Fig. 3 – Residuals for PGA and PGV versus V_{S30}

In order to quantitatively analyze the congruence between observed and simulated PSA, we compute the observed-to-simulated model standard deviation and bias. The standard deviation is defined as

$$\sigma(T) = \sqrt{\frac{1}{N} \sum_{i=1}^N \{ \ln O_i(T) - \ln S_i(T) - B(T) \}^2} \tag{12}$$

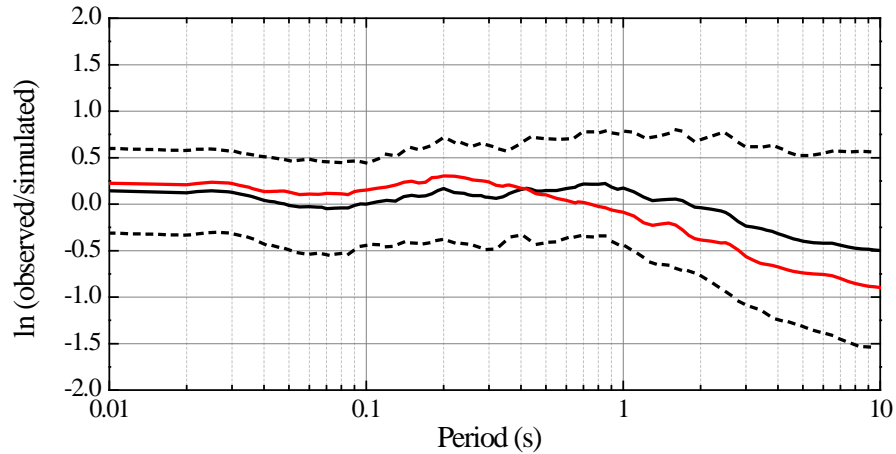


Fig. 4 – Model bias (black solid line) and standard deviation (dashed lines) averaged over all stations. Red solid line denotes the corresponding model bias for simulation using constant radiation pattern.

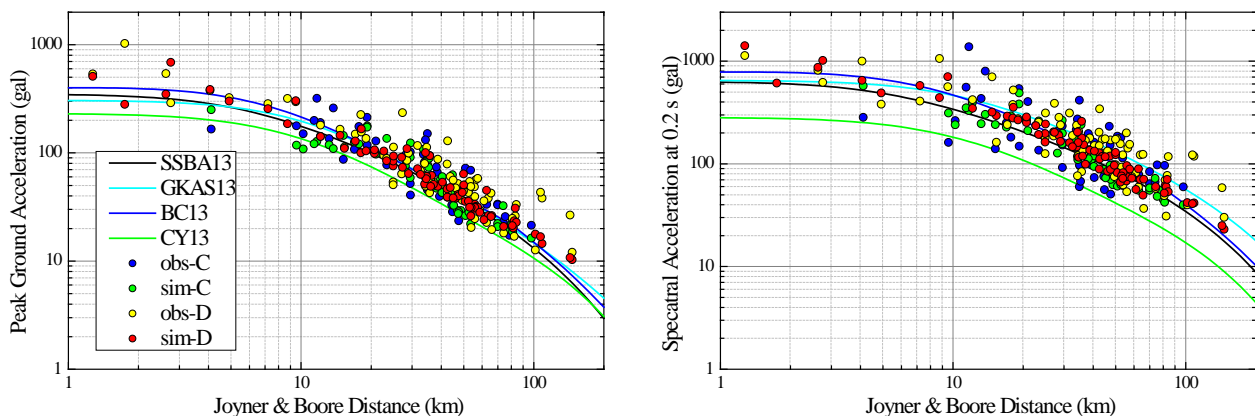
where N is the number of stations, $O_i(T)$ and $S_i(T)$ represent the observed and simulated PSA at the period T of the i th station, and $B(T)$ is the model bias given by

$$B(T) = \frac{1}{N} \sum_{i=1}^N \{ \ln O_i(T) - \ln S_i(T) \} \quad (13)$$

Then, the model bias and standard deviation averaged over all stations are plotted in Fig.4. It can be seen that the observed and simulated PSA at periods below 2 s are in reasonable agreement with little discreteness in a statistical sense, proving that the kappa value of 0.035 can represent the average vertical kappa value of all the selected stations although some difference existed in kappa between soil and rock sites. Compared to the constant radiation pattern, the direction-dependent radiation pattern model contributes to better estimation of PSA for both short and long periods, suggesting that the inclusion is preferable. The reason for the underestimation of PSA above 2 s is due to the inherent deficiencies of stochastic method [18].

4. Comparison with vertical GMPEs

In this section, the simulated vertical records are further validated by four vertical GMPEs [44] (referred to as SSBA13, GKAS13, BC13 and CY13, respectively) developed from the PEER NGA-West2 database. As depicted in Fig.3, the numbers of stations for different site classes are 62 and 81 for C and D while only 2, 1 for B and E, thus in this part we only adopt stations belong to sites C and D for brevity. Considering the average of site conditions, the boundary of sites C and D, namely, generic soil site with V_{S30} of 360 m/s, is chosen to depict four vertical GMPEs for Northridge earthquake. Then, the observed and simulated PGA and PSA at 0.2 s, 1.0 s and 2.0 s are compared with vertical GMPEs, respectively, as shown in Fig.5.



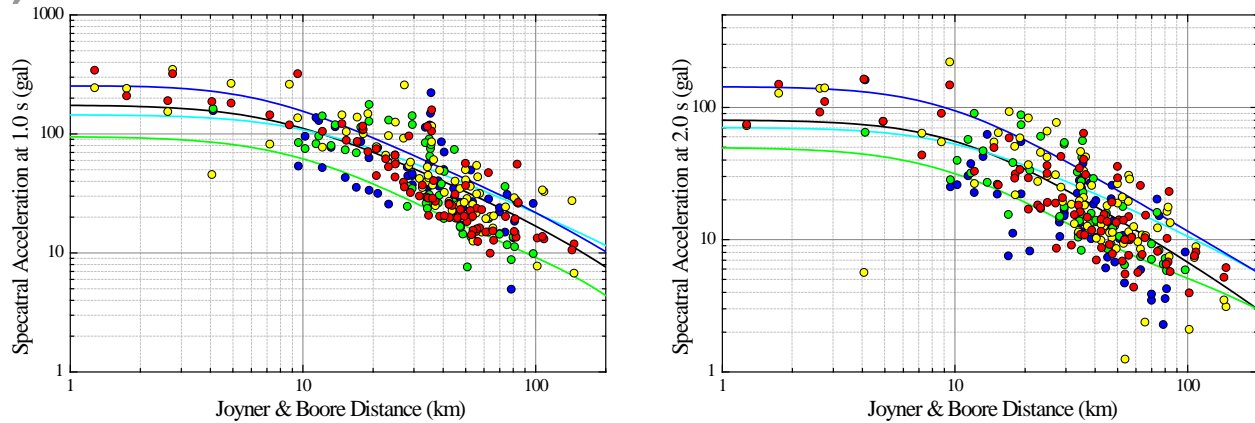


Fig. 5 – Comparison of observed and simulated PGA and PSA at 0.2 s, 1.0 s and 2.0 s with four vertical GMPEs for the 1994 Northridge earthquake

From the comparisons, we can see that observed and simulated PGAs are in good accordance, especially for PGA. Moreover, there are no systematic differences between sites C and D. Combined with the result of model bias, it is evident that the comparisons of PSA at 0.2 s are similar with that of PGA. There is an obvious trend that the deviation increases with period. Similar analysis shows that the comparison for the PSA at 0.2 s is equally applicable to that for the PSA at short periods of most engineering interest, as we expected from Fig.4. In addition, CY13 predicts obviously lower values than the other three GMPEs for the Northridge earthquake.

5. Conclusion

From the engineering requirements of vertical ground motions, we discuss the necessity to extend stochastic simulation for vertical ground motion as seismic code and vertical GMPEs cannot meet the need satisfactorily. Then, the stochastic method is investigated in detail to evaluate the direction-dependence of each term, and we conclude that stress parameter and quality factor are only region-specific parameters, which indicates the independence of source effect and path effect on direction. The obvious direction-dependence is expressed by two key terms of site effects, kappa factor and site amplification. Thus, specific value for vertical kappa factor is adopted from the fact that vertical kappa value is systematically smaller than horizontal one, site amplification models for sites C and D and generic rock site are employed by correcting the horizontal counterparts with empirical correction factors. In addition, the scaling factor C loses vital opportunity to express directions because of the constant radiation pattern. Thus, based on Pulido's researches, direction-dependent radiation pattern is incorporated into EXSIM with our improvements. Afterwards, taking the 1994 Northridge earthquake as an example for validation, we find the simulated PGA and PGV are in good accordance with the observed value. Model bias of PSA for short periods of most interest is quite small with little discreteness in a statistical sense. Furthermore, the observed and simulated PGA and PSA at 0.2 s, 1.0 s and 2.0 s also coincide well with recently developed vertical GMPEs. These analyses demonstrate that the incorporation of direction-dependent parameters for vertical direction into stochastic method is a practical way to simulate vertical ground motion.

6. Acknowledgements

The records of the 1994 Northridge earthquake are obtained from the PEER NGA-West2 database (<http://ngawest2.berkeley.edu/>) for research applications. The slip model of the Northridge earthquake is available through the Finite-Source Rupture Model Database at the website eQuake-RC (<http://equake-rc.info/>). The code of stochastic finite-fault simulation is accessed from Dr. Dariush Motazedian's website (<http://www.carleton.ca/~dariush>). The authors thank Dr. Dilli Ram Thapa for providing language help.



7. References

- [1] Kunnath SK, Erduran E, Chai YH, Yashinsky M (2008): Effect of near-fault vertical ground motions on seismic response of highway overcrossings. *Journal of Bridge Engineering*, **13** (3), 282-290.
- [2] Gülerce Z, Abrahamson NA (2011): Site-specific design spectra for vertical ground motion. *Earthquake Spectra*, **27** (4), 1023-1047.
- [3] Bozorgnia Y, Niazi M, Campbell KW (1995): Characteristics of free-field vertical ground motion during the Northridge earthquake. *Earthquake spectra*, **11** (4), 515-525.
- [4] Papazoglou AJ, Elnashai AS (1996): Analytical and field evidence of the damaging effect of vertical earthquake ground motion. *Earthquake Engineering & Structural Dynamics*, **25** (10), 1109-1138.
- [5] Beresnev IA, Nightengale AM, Silva WJ (2002): Properties of vertical ground motions. *Bulletin of the Seismological Society of America*, **92** (8), 3152-3164.
- [6] Bozorgnia Y, Campbell KW (2004): The vertical-to-horizontal response spectral ratio and tentative procedures for developing simplified V/H and vertical design spectra. *Journal of Earthquake Engineering*, **8** (02), 175-207.
- [7] Bommer JJ, Akkar S, Kale Ö (2011): A model for vertical-to-horizontal response spectral ratios for Europe and the Middle East. *Bulletin of the Seismological Society of America*, **101** (4), 1783-1806.
- [8] GB 50011-2010 (2010): *Code for seismic design of buildings*. China Architecture & Building Press. (in Chinese)
- [9] NZS 1170.5-2004 (2004): *Structural design actions, Part 5: earthquake actions-New Zealand*. Standard New Zealand.
- [10] Eurocode 8 (2005): *Design of structures for earthquake resistance-Part 1: General rules, seismic actions and rules for buildings*. European Committee for Standardization.
- [11] Building Seismic Safety Council (2009): *NEHRP recommended seismic provisions for new buildings and other structures (FEMA P-750)*. Federal Emergency Management Agency.
- [12] Bozorgnia Y, et al. (2014): NGA-West2 research project. *Earthquake Spectra*, **30** (3), 973-987.
- [13] Akkar S, Sandikkaya MA, Ay BÖ (2014): Compatible ground-motion prediction equations for damping scaling factors and vertical-to-horizontal spectral amplitude ratios for the broader Europe region. *Bulletin of earthquake engineering*, **12** (1), 517-547.
- [14] Olsen KB, Archuleta RJ, Matarese JR (1995): Three-dimensional simulation of a magnitude 7.75 earthquake. *Science*, **270**, 1628-1632.
- [15] Pitarka A, Somerville P, Fukushima Y, Uetake T, Irikura K (2000): Simulation of near-fault strong-ground motion using hybrid Green's functions. *Bulletin of the Seismological Society of America*, **90** (3), 566-586.
- [16] Graves RW, Pitarka A (2010): Broadband ground-motion simulation using a hybrid approach. *Bulletin of the Seismological Society of America*, **100** (5A), 2095-2123.
- [17] Boore DM (1983): Stochastic simulation of high-frequency ground motions based on seismological models of the radiated spectra. *Bulletin of the Seismological Society of America*, **73** (6A), 1865-1894.
- [18] Boore DM (2003): Simulation of ground motion using the stochastic method. *Pure and applied geophysics*, **160** (3-4), 635-676.
- [19] Beresnev IA, Atkinson GM (1998): FINSIM--a FORTRAN program for simulating stochastic acceleration time histories from finite faults. *Seismological Research Letters*, **69** (1), 27-32.
- [20] Motazedian D, Atkinson GM (2005): Stochastic finite-fault modeling based on a dynamic corner frequency. *Bulletin of the Seismological Society of America*, **95** (3), 995-1010.
- [21] Joshi A, Kumar P, Kumar A (2014): Effect of frequency-dependent radiation pattern in the strong motion simulation of the 2011 Tohoku earthquake, Japan, using modified semi-empirical method. *Natural Hazards*, **73** (3), 1499-1521.
- [22] Aki K, Richards PG (2002): *Quantitative seismology: theory and methods*. University science books, 2nd edition.
- [23] Ben-Menahem A, Smith SW, Teng TL (1965): A procedure for source studies from spectrums of long-period seismic body waves. *Bulletin of the Seismological Society of America*, **55** (2), 203-235.



- [24] Boore DM, Boatwright J (1984): Average body-wave radiation coefficients. *Bulletin of the Seismological Society of America*, **74** (5), 1615-1621.
- [25] Pulido N, Kubo T (2004): Near-fault strong motion complexity of the 2000 Tottori earthquake (Japan) from a broadband source asperity model. *Tectonophysics*, **390** (1), 177-192.
- [26] Pulido N, Ojeda A, Atakan K, Kubo T (2004): Strong ground motion estimation in the Sea of Marmara region (Turkey) based on a scenario earthquake. *Tectonophysics*, **391** (1), 357-374.
- [27] Pulido N, Dalguer LA (2009): Estimation of the high-frequency radiation of the 2000 Tottori (Japan) earthquake based on a dynamic model of fault rupture: application to the strong ground motion simulation. *Bulletin of the Seismological Society of America*, **99** (4), 2305-2322.
- [28] Liu HL, Helmberger DV (1985): The 23: 19 aftershock of the 15 October 1979 Imperial Valley earthquake: more evidence for an asperity. *Bulletin of the Seismological Society of America*, **75** (3), 689-708.
- [29] Vidale JE (1989): Influence of focal mechanism on peak accelerations of strong motions of the Whittier Narrows, California, earthquake and an aftershock. *Journal of Geophysical Research: Solid Earth (1978–2012)*, **94** (B7), 9607-9613.
- [30] Satoh T (2002): Empirical frequency-dependent radiation pattern of the 1998 Miyagiken-Nanbu earthquake in Japan. *Bulletin of the Seismological Society of America*, **92** (3), 1032-1039.
- [31] Castro RR, et al. (2006): Analysis of the frequency dependence of the S-wave radiation pattern from local earthquakes in central Italy. *Bulletin of the Seismological Society of America*, **96** (2), 415-426.
- [32] Brune JN (1970): Tectonic stress and the spectra of seismic shear waves from earthquakes. *Journal of geophysical research*, **75** (26), 4997-5009.
- [33] Atkinson GM, Beresnev I (1997): Don't call it stress drop. *Seismological Research Letters*, **68** (1), 3-4.
- [34] Aki K (1980): Attenuation of shear-waves in the lithosphere for frequencies from 0.05 to 25 Hz. *Physics of the Earth and Planetary Interiors*, **21** (1), 50-60.
- [35] Atkinson GM, Boore DM (1995): Ground-motion relations for eastern North America. *Bulletin of the Seismological Society of America*, **85** (1), 17-30.
- [36] Anderson JG, Hough SE (1984): A model for the shape of the Fourier amplitude spectrum of acceleration at high frequencies. *Bulletin of the Seismological Society of America*, **74** (5), 1969-1993.
- [37] Ktenidou OJ, Cotton F, Abrahamson NA, Anderson JG (2014): Taxonomy of κ : A review of definitions and estimation approaches targeted to applications. *Seismological Research Letters*, **85** (1), 135-146.
- [38] Motazedian D (2006): Region-specific key seismic parameters for earthquakes in Northern Iran. *Bulletin of the Seismological Society of America*, **96** (4A), 1383-1395.
- [39] Sun X, Tao X, Duan S, Liu C (2013): Kappa (κ) derived from accelerograms recorded in the 2008 Wenchuan mainshock, Sichuan, China. *Journal of Asian Earth Sciences*, **73**, 306-316.
- [40] Raghukanth STG, Somala SN (2009): Modeling of strong-motion data in northeastern India: Q, stress drop, and site amplification. *Bulletin of the Seismological Society of America*, **99** (2A), 705-725.
- [41] Askan A, Sisman FN, Pekcan O (2014): A regional near-surface high frequency spectral attenuation (kappa) model for northwestern Turkey. *Soil Dynamics and Earthquake Engineering*, **65**, 113-125.
- [42] Ktenidou OJ, Gélis C, Bonilla LF (2013): A study on the variability of kappa (κ) in a borehole: implications of the computation process. *Bulletin of the Seismological Society of America*, **103** (2A), 1048-1068.
- [43] Zhao JX, et al. (2006): An empirical site-classification method for strong-motion stations in Japan using H/V response spectral ratio. *Bulletin of the Seismological Society of America*, **96** (3), 914-925.
- [44] Gülerce Z, et al. (2013): NGA-West2 Ground motion prediction equations for vertical ground motions. *Technical Report PEER 2013/24*, Pacific Earthquake Engineering Research, Berkeley, USA.
- [45] Boore DM, Joyner WB (1997): Site amplifications for generic rock sites. *Bulletin of the seismological society of America*, **87** (2), 327-341.



- [46] Boore DM (2016): Determining generic velocity and density models for crustal amplification calculations, with an update of the Boore and Joyner (1997) generic site amplification for $V_S(Z)=760$ m/s. *Bulletin of the Seismological Society of America*. (in press)
- [47] Ancheta TD, et al. (2014): NGA-West2 database. *Earthquake Spectra*, **30** (3), 989-1005.
- [48] Wald DJ, Heaton TH, Hudnut KW (1996): The slip history of the 1994 Northridge, California, earthquake determined from strong-motion, teleseismic, GPS, and leveling data. *Bulletin of the Seismological Society of America*, **86** (1B), S49-S70.
- [49] Beresnev IA, Atkinson GM (2002): Source parameters of earthquakes in eastern and western North America based on finite-fault modeling. *Bulletin of the Seismological Society of America*, **92** (2), 695-710.
- [50] Beresnev IA, Atkinson GM (1999): Generic finite-fault model for ground-motion prediction in eastern North America. *Bulletin of the Seismological Society of America*, **89** (3), 608-625.